Cryobiology 103 (2021) 32–38

Contents lists available at ScienceDirect

Cryobiology

journal homepage: www.elsevier.com/locate/cryo

Infrared thermal imaging controls freezing and warming in skin cryoablation

Gennadiy O. Kovalov [a,*], Galyna V. Shustakova [b], Eduard Yu. Gordiyenko [b], Yuliya V. Fomenko [b], Mykola I. Glushchuk [b]

[a] Institute for Problems of Cryobiology and Cryomedicine of the National Academy of Sciences of Ukraine, Postal address: 23, Pereyaslavska str., Kharkiv, 61016, Ukraine

[b] B. Verkin Institute for Low Temperature Physics and Engineering of the National Academy of Sciences of Ukraine, Postal address: 47 Nauky Ave., Kharkiv, 61103, Ukraine

ARTICLE INFO

Keywords:
Cryosurgery
Skin
Freezing
Warming
Temperature field dynamics
Infrared thermography

ABSTRACT

The purpose of this study was to assess the possibilities of intraoperative control of the current parameters of frozen biological tissues in the cryoablation area, including the instant location of primary necrosis isotherm, based on the dynamics of thermal fields on skin surface. Cryoablation of skin was performed in 30 rats with exposure durations of 0.5, 1 and 2 min. The contact cryoprobe actively cooled with liquid nitrogen was used. The dynamics of animal's skin thermal field during freeze/thaw cycle was quantitatively controlled by the original infrared camera with an extended range of measurable temperatures. The obtained by us ratio of the maximal diameters of primary necrosis and ice spots was 0.64 ± 0.03 for cryoexposure durations of 0.5 and 1 min. During thawing, a quasi-stable stage was observed both in the dynamics of ice spot diameters and their temperature distribution. The effect is presumably associated with structural rearrangements of ice in the frozen tissue volume. The results indicate that thermal imaging can be effectively used for quantitative control of freezing and warming of biological tissues *in vivo*, including current control of the position of necrotic and cryoscopic isotherms, distortion of their thermal symmetry, thermal response of other skin areas, etc.

1. Introduction

Cryoablation is a well-known technique widely used in skin surgery due to convenient access and visualization of surgical field, as well as the relative ease of post-surgery care due to the anatomical features of an organ. More than 80 dermatological diseases are amenable to cryosurgery treatment [1]. Among these diseases there are benign neoplasms (hemangiomas, dermatofibromas, molluscum contagiosum, keloids and hypertrophic scars, common, plantar, flat warts, etc.), precancerous lesions (actinic keratosis, Bowen's foci, keratoacanthomas, lentigo maligna, etc.) as well as some types of malignant tumors (basal cell and squamous cell carcinomas). Also, cryosurgery is used to treat purulent wounds, local inflammatory processes, viral skin lesions, etc.

Planning the surgery, it is very important to strike a balance between the drastic cryodestruction and healthy tissues maximal intactness. The efficiency of pathological tissue cryoablation directly depends on the size and temperature of the freezing zone, exposure duration, the speed of freezing/warming processes [13]. Besides, the freezing area parameters depend on the individual patient features such as age, skin and vascular system condition, pathology localization (for example, near a large blood vessel). Assuming this fact, surgeons overly include surrounding tissues in the cryodestruction zone to avoid tumor relapse. Therefore, intraoperative monitoring of the boundaries of the zone of irreversible tissue damage (primary necrosis) caused by the cooling temperature $T \leq T_{nec}$ is very important. Also, monitoring the growing freezing area with a temperature of $T \leq T_{cr}$, where T_{cr} is the cryoscopic temperature of a specific tissue, is required. This control is especially important if damage to adjacent tissues (e.g., face, genitals) can lead to serious functional or cosmetic problems.

"The future of cryosurgery is intricately related to imaging techniques in progress; particularly those for *in vivo* real-time use" [1, P. 749]. Generally accepted clinical imaging techniques (MRI, ultrasound and CT) can be used for the cryoablation planning and for post-surgery monitoring. However, these methods are difficult to use directly during

* Corresponding author.
E-mail addresses: g.o.kovalyov@nas.gov.ua (G.O. Kovalov), shustakova@ilt.kharkov.ua (G.V. Shustakova), gordiyenko@ilt.kharkov.ua (E.Yu. Gordiyenko), yufomenko@ilt.kharkov.ua (Y.V. Fomenko), glushchuk@ilt.kharkov.ua (M.I. Glushchuk).

https://doi.org/10.1016/j.cryobiol.2021.09.014
Received 7 June 2021; Received in revised form 16 September 2021; Accepted 27 September 2021
Available online 11 October 2021

cryoablation, especially on an outpatient basis. It is the well-known fact that ultrasound technique is used for intraoperative control of the frozen zone size [9,15], however, additional contact probe (ultrasonic sensor) interferes the surgeon activity. Also, ultrasound does not provide information on the temperature distribution in the area of interest. A promising method of MRI thermometry [10] makes it possible to measure internal thermal fields by analyzing temperature dependences of MRI some parameters. This is exemplified by the results of MRI thermometry of frozen pig muscles during cryoablation *ex vivo* [12]. With three-dimensional ultrashort echo time (3D UTE) imaging, MRI temperature maps were obtained, the values of which were in good agreement with the readings of the control temperature sensors within the range up to −40 °C. However, this can be hardly accomplished and is quite expensive in practice. Typically, in both clinical practice and most of research, one or two miniature thermocouples are placed in the target area to control the temperature [5,6]. For example the thermocouple fixes the moment when the boundary of freeze or necrosis zone reaches this point. However, single thermocouples do not provide information about the temperature distribution over the entire area of interest. In addition, thermocouple long wires in operative field interfere the surgeon as well as distort the thermal field symmetry because of heat gain.

In this study, we have used the functional non-invasive infrared (IR) thermal imaging [4] for intraoperative remote monitoring of thermal field dynamics *in vivo*. As early as 1996, IR thermal imaging was successfully used during cryosurgery in eight rat abdomen with a liquid nitrogen cryoprobe in a triple-freeze technique [14] to accurately predict the volume of soft tissue necrosis. However, the researchers concluded that the thermal imaging equipment existed at that time was impossible to use clinically because of its non-general availability, high cost, and complexity.

Modern IR cameras have high spatial resolution, temperature sensitivity, and speed, which allow analyzing fast processes with high accuracy. They are also compact, relatively cheap, uncomplicated image analysis, and do not require special technical or computer skills. However, till now this promising method of clinical imaging is rarely used in cryomedicine because of the poorly studied pathophysiological basis of thermal images as well as the lack of clinical protocols with quantitative thermal image analysis. Further obstacle to use thermal imagers in cryosurgery is impossibility to measure negative temperatures lower than −20 °C, which is common for most commercial devices. This range is sufficient to control the temperatures required to destroy the most of benign neoplasm, but insufficient for malignant neoplasms with $T_{nec} \leq -40$ °C [13,20]. So there is a serious limitation on using standard IR thermal imagers for real-time control of the movement of the tissue necrosis zone boundaries.

IR radiation with a wavelength of more than 3 microns does not almost penetrate into biological tissues. Therefore medical thermal imagers operating within spectral sensitivity range of 7–14 microns, perceive thermal fields on the skin surface and at a depth of less than 0.1 mm only.

In accordance with the computational model [16], the volume of tissues frozen with a penetrating point cryoprobe has a spherical shape with a radial temperature distribution. The frozen zone volume caused by exposure on the surface with contact quasi-point cryoapplicator was mathematically modeled by a hemisphere and confirmed experimentally in model fluid [7].

It is known that the rate of tissue cooling is a significant factor affecting the activity of metabolic processes in cells, and at low temperatures the rate of chemical reactions is so low that metabolic processes in cells practically stop [2,17]. Since we froze tissues at a high rate to low temperatures, it is obvious that the individual characteristics of metabolism within the frozen zone could be neglected.

In view of the above, our study is based on two assumptions:

1. The round ice spot on the skin surface caused by point cryoapplicator is considered as a diametrical cross section of the hemispheric frozen tissue volume. Radial temperature distribution in the ice spot on the surface corresponds to the one in the ice hemisphere volume. In this case, real-time monitoring of thermal field dynamics on skin provides quantitative values of the frozen bulk tissue, including both the frozen as well as necrosis volume and depth at any moment of freeze/thaw cycle.
2. The instantaneous thermal field distribution inside the frozen zone is determined only by the temperature-dependent thermophysical parameters of this type of tissue. Then the instantaneous position of the isotherm of primary necrosis (critical isotherm in some publications) can be estimated by measuring the simultaneous location of higher-temperature isotherms, for example, cryoscopic one.

The possibility of intraoperative IR monitoring of the dynamics of the frozen zone and the one of primary tissue necrosis in a healthy rat with short-term (0.5 min) skin cryoablation has been previously demonstrated by us [8]. The maximal diameters of the cryoscopic isotherm and primary necrosis one measured in those experiments did not exceed 20 mm and 13 mm, respectively. During natural warming, a long quasi-stable stage was observed in the dynamics of cryoscopic isotherms with an insignificant change in the frozen zone temperature field.

The purpose of this study was to assess the possibilities of intraoperative control of the current parameters of frozen biological tissues in the cryoablation area, including the instant location of primary necrosis isotherm, based on the dynamics of thermal fields on skin surface.

2. Materials and methods

2.1. Cryoprobe

The designed at the Institute for Problems of Cryobiology and Cryomedicine of the National Academy of Sciences of Ukraine, contact cryoprobe actively cooled by liquid nitrogen, have been used for cryoablation. The cryoprobe copper tip with 8 mm diameter of and 1 mm thickness is considered a point source of cold for the animal. The tip temperature measured by a copper-constantan thermocouple prior contact with skin was (−192.0 … −194.8) °C.

2.2. Animal groups

The study was carried out in 6-month-old white male rats (30 animals) weighing 230–260 g following the requirements of the Bioethics Committee at Institute for Problems of Cryobiology and Cryomedicine of the National Academy of Sciences of Ukraine (protocol № 5 dated 08.12.2020) in accordance with the EU Directive 2010/63/EU for animal experiments.

The Telazol (Zoetis Inc., USA) was used at a dose of 50 mg/kg intramuscularly to anesthetize the animals. The animal with the hair removed (by dry depilation) in the areas under the study was fixed on a horizontal heat insulating surface with back up. Cryoablation was performed by cryoprobe tip contact with the skin in lateral thigh surface for 0.5 min (10 animals), 1 min (10 animals), and 2 min (10 animals).

After the end of the thermography the rats were sacrificed immediately while under anesthesia.

2.3. IR camera

This research involved the passive IR thermal imaging was used [4]. The original IR camera based on a single-element semiconductor detector cooled down to the liquid nitrogen temperatures has been used. The model was developed at the B. Verkin Institute for Low Temperature Physics and Engineering of the NAS of Ukraine using the concept presented in Ref. [18] earlier.

The camera distinctive feature is the range of measured negative temperatures expanded to boiling point of liquid nitrogen. To reduce the error of low temperature measuring, the special reference emitter (a

metal shutter) was introduced into the device optical channel. A thin layer of aluminum is sprayed onto the surface of the shutter, which provides an effective reflection of IR radiation in a wide spectral range (reflection coefficient ≈ 95%). At the end of each frame, the field of view of the system is completely shut by a mirror shutter so that only the reflected radiation flux, created by the detector itself and its cooled aperture diaphragm, reaches the detector. The liquid nitrogen-cooled detector has a fixed temperature during operation. Therefore, the used shutter can be considered as a reference emitter with a stable temperature equal to the boiling point of liquid nitrogen. The temperature of the observed objects is calculated using the software relative to the reference emitter temperature.

The camera was calibrated within the temperature range (−30 … +50) °C using metrological bench Fluke Portable Infrared Calibrator-9133 (Fluke Corporation, USA). The accuracy of absolute temperature measuring is estimated as ± 1 °C within the range (−30 … 0) °C, and ±0.5 °C in the range (0 … +50) °C. The camera was calibrated in the range (−196 … −30) °C using a blackbody model, the temperature of which was controlled by a copper-constantan thermocouple. We assume the accuracy of measuring the absolute temperature in this range as ± 3 °C, based on the manual instruction data for the copper-constantan thermocouple. Other parameters of the developed camera are as follows: temperature sensitivity 0.1 °C, spatial resolution 1.5 mrad, time of frame 1.5 s, field of view (22H × 22 V) deg. The software was optimized for this research, including a continuous sequence of digital image frames was automatically recorded during half an hour for observation of the object thermal field dynamics (thermographic movie).

2.4. Experiment and data processing

The IR camera was placed at a distance of 1 m from the area of interest with a constant tilt angle. A temperature of the blackbody model located near the animal was used as a reference for absolute temperature measurement and environment condition control. A thermocouple located on the reverse side of the animal thigh fixed the moment of equality of the frozen depth and the animal thigh thickness. In some experiments, an additional thermocouple was attached on the upper skin surface in the area of interest. To simplify the quantitative analysis, we considered $T_{cr} = 0°C$, since the difference between the freezing temperature of pure water and of the tissue under the study (≈−0.6°C [13]) does not exceed the error of absolute temperature measurement by any IR imaging camera. We used the value of the necrosis temperature $T_{nec} \leq -20°C$ for this type of tissue [14]. The quantitative processing of the digital data array of each frame of the thermal imaging movie was carried out using the original software. Fig. 1 shows a block diagram of the experiment and Fig. 2 demonstrates the user interface of original software with the thermal animal image at warming.

Further data were processed by primary statistical analysis using the Excel 2010 software (Microsoft, USA). The results are presented as M ± S, where M is the sample mean for the group parameter value, S is the standard deviation. The significance of differences was assessed by the Kruskal-Wallis test ($p < 0.05$) using the Statistica 10 software (StatSoft, USA).

3. Results and discussion

3.1. Ice spot dynamics

The typical time dependencies of ice spot diameters during various cryoexposure duration and subsequent natural warming are represented in Fig. 3. Using original software, current cryoscopic isotherms were measured with an accuracy of ±0.5 mm by the coordinates of two opposite image pixels with the temperature T ≈ 0 °C located on the temperature profile drawn through the spot center. Using these temperature profiles, the dynamic of the temperature distribution inside and outside the ice spots was analyzed as well as the current primary

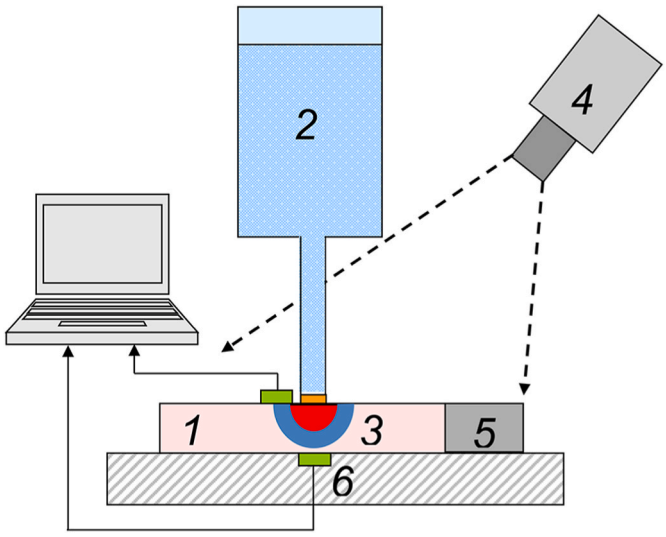

Fig. 1. Experimental diagram: 1 – animal, 2 – contact cryoprobe, 3 - ice hemisphere and primary necrosis area, 4 – IR camera, 5 – blackbody, 6 - thermocouple.

necrosis isotherm with $T_{nec} = -20°C$ was measured. The moment of ice spot finish thawing was fixed when the minimal temperature (usually in the ice spot center) reached the value $T_{min} = 0°C$.

The ice spot diameters can be found to increase to various maximal values depending on exposure duration. The further process of thawing in natural conditions may be roughly divided into three stages:

- initial short-term diameter decrease;
- long-term quasi-stable diameter state;
- diameter final reduction up to a complete ice melting.

It should be noted that ice spot diameters reach some minimum before the quasi-stable stage (QSS) beginning for all 20 animals exposed to 1 and 2 min. The authors explain this effect of the cryoprobe tip mechanical indentation into tissues, followed by their deep freezing. The IR camera sees only the bottom of cryoprobe-initiated frozen invagination of tissue until the skin comes back to initial state. The longer the cryoexposure, the longer the invagination is kept. Such an effect is not observed in any of the 10 animals exposed by 0.5 min cryoablation.

The typical behavior of ice spot minimal temperatures T_{min} during natural warming after various cryoexposure durations is illustrated in Fig. 4. Similarly to the dynamics of the ice spot diameters, three characteristic stages can be distinguished on the minimal temperature-time dependencies:

- initial rapid temperature rising from cryogenic to some intermediate values;
- quasi-stable temperature with light linear growth within the period dependent on cryoexposure duration;
- subsequent temperature rising till the passage of the point of complete ice melting at the time moment dependent on the cryoexposure duration, and further long (several hours) period of warming.

It can be seen correspondence in the characteristic stage existence as well as coincidence in the moments of their changes between the two processes, shown in Figs. 3 and 4. The results of comparing these time dependencies at various cryoexposure durations are shown in Fig. 5.

The dependencies in Fig. 5 show the presence of QSS with comparable duration in both processes: ice spot diameter decreases and its temperature increases. Thus during QSS, the ice hemisphere, without noticeable changes in its size and temperature, absorbs significant heat gains from the blood flow and exothermic metabolic reactions of tissues

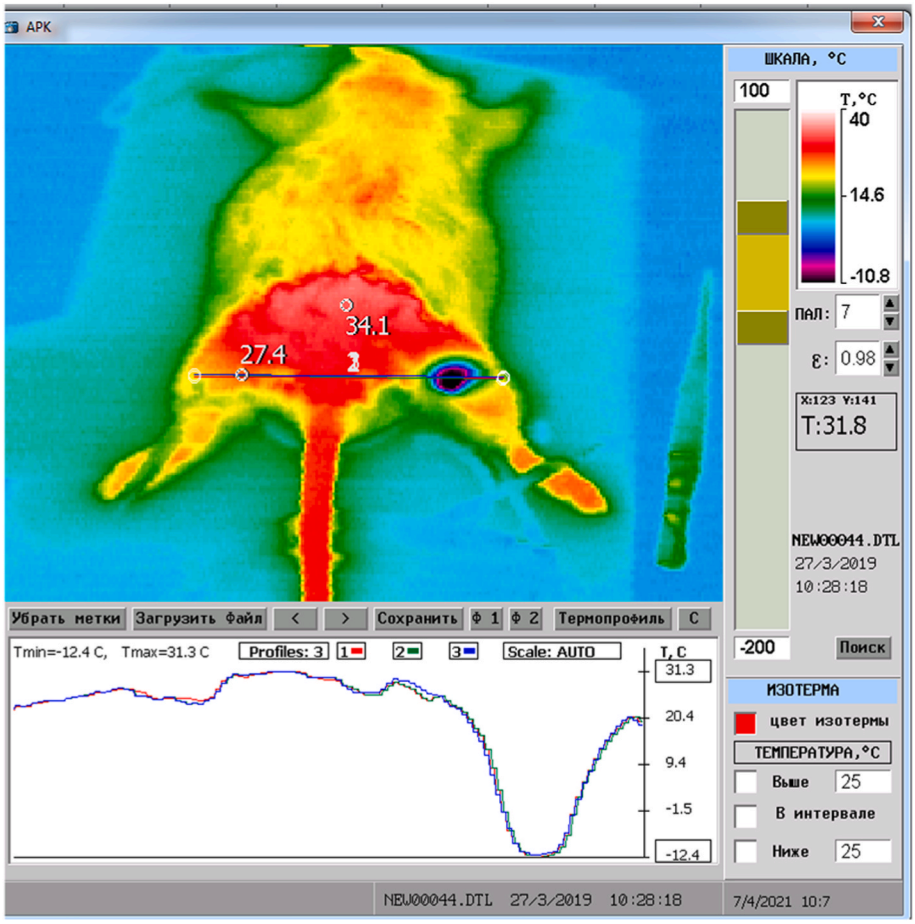

Fig. 2. User interface with IR image of animal during warming.

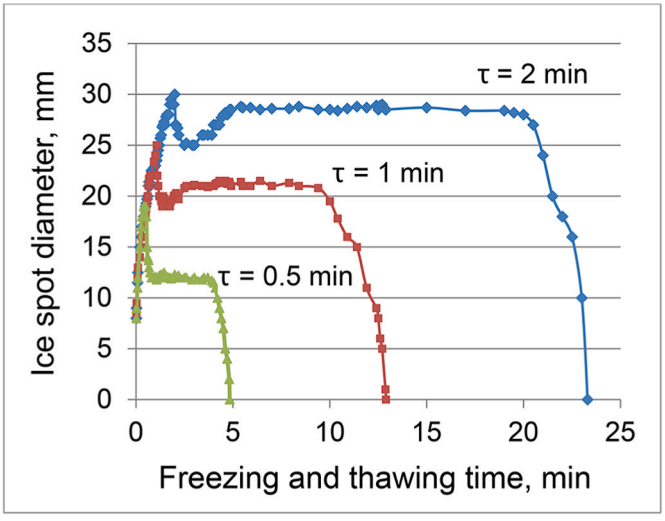

Fig. 3. Dynamic of ice spot diameters at various cryoexposure durations and subsequent warming.

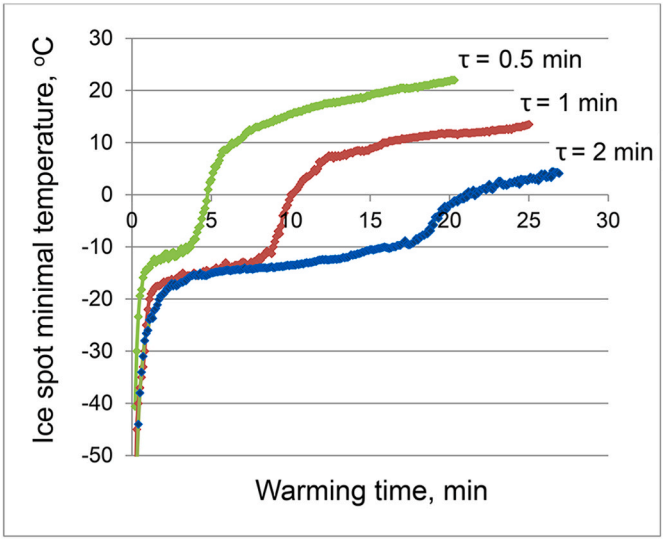

Fig. 4. Typical behavior of ice spot minimal temperatures during natural warming after various cryoexposure durations.

surrounding the frozen area, as well as heat gains from the external environment, which heat the ice spot through radiation and convection.

The thermodynamical approach indicates the first-order phase transition. Presumably, observable effect is associated with structural changes in the ice composition, including recrystallization processes [19].

3.2. Statistical analysis

The ice spot parameters during warming were processed by the primary statistics methods and Kruskal-Wallis test for three groups of animals are shown in Table. The Table shows the time parameters, obtained after the moment of the cryoprobe tip was removed from the skin

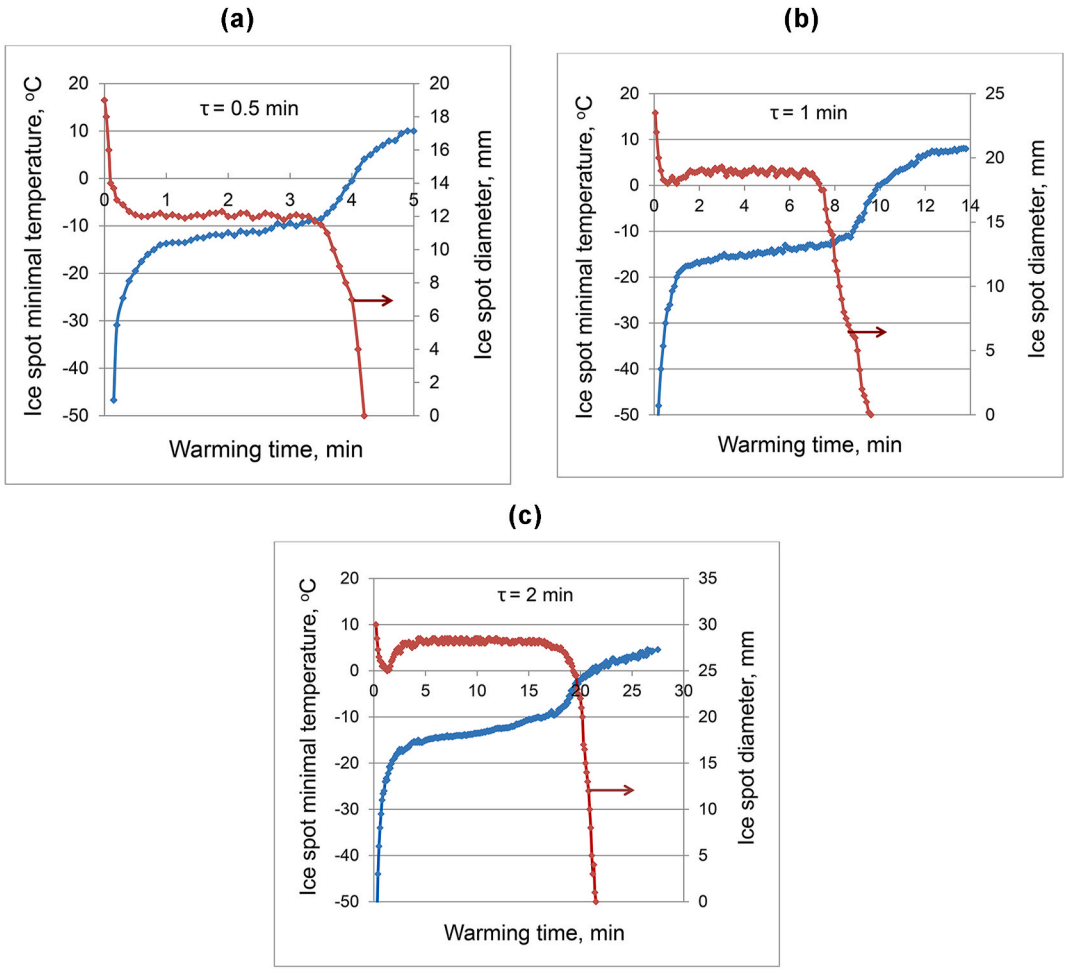

Fig. 5. Dynamics of ice spot diameters and their minimal temperatures during warming after cryoexposure durations: a) τ = 0.5 min, b) τ = 1 min, c) τ = 2 min.

surface. The time parameters of the QSS (beginning, end, duration) are estimated by the interval in which the dependence is approximated by a linear function. The results are presented as M ± S, where M is the average group value of the parameter, S is the standard deviation, and n is the number of subjects in a group. The asterisk (*) indicates significant difference between the group parameter compared analogous parameter of the group 1, and the # - of the group 2.

Table 1
Ice spot parameters measured during thawing for animal groups under study.

Measured parameter	Group 1	Group 2	Group 3
Max. diameter of ice spot, mm	18.54 ± 1.00	23.66 ± 1.29*	28.35 ± 1.06*#
Max. diameter of necrosis spot, mm	11.91 ± 0.82	15.10 ± 1.15*	18.30 ± 0.82*#
Diameter of ice spot in QSS, mm	11.74 ± 0.93	19.52 ± 2.05*	25.72 ± 1.18*#
QSS start time, min	0.87 ± 0.20	2.13 ± 0.30*	1.75 ± 0.26*
QSS duration (on diameter), min	2.51 ± 0.47	5.13 ± 0.32*	10.83 ± 1.33*#
QSS duration (on temperature), min	2.37 ± 0.33	5.04 ± 0.56*	10.32 ± 1.52*#
Temperature at QSS beginning, °C	−12.74 ± 0.73	- 16.64 ± 0.66*	−13.95 ± 1.31#
Full thawing time, min	4.18 ± 0.35	10.89 ± 0.86*	20.18 ± 2.18*#
Calculated parameter			
Necrosis to ice diameters ratio	0.64 ± 0.02	0.64 ± 0.03	0.65 ± 0.03
Temperature rise in QSS, °C/min	1.85 ± 0.25	0.56 ± 0.10*	0.37 ± 0.08*

The results of the Kruskal-Wallis test demonstrate (see Table 1) the significant differences of the parameters of group 2 compared to corresponded ones for group 1, that indicates the influence of freezing duration on ice spot parameters. However, the expected differences of some QSS parameters of group 3 compared to corresponding parameters of other groups are not observed. An example of such unexpected behavior of ice spot temperature in QSS for a rat from group 3 can be seen in Fig. 4, i.e. the dependence practically coincides with ice spot temperature dynamic for an animal from group 2. The authors assume that observed absence of significant differences in some parameters of group 3 compared to other groups is explained by small thickness of the rat's thigh (10–13 mm). With cryoablation for 2 min, the animal thigh freezes through, which is confirmed by the readings of a thermocouple located under the thigh in the projection of the cryoapplicator center (see the block diagram in Fig. 1). At some point in cryoablation, the radius of the ice hemisphere becomes greater than the thigh thickness. This leads to truncating of the ice hemisphere, changes the conditions of thermodynamic equilibrium and, accordingly, the parameters of structural rearrangement of ice.

It should also be noted that for animals of group 3 and group 2, the radius of the ice spot on the surface, measured at the moment when the ice front reaches the under-thigh thermocouple (T = 0 °C), is approximately equal to the thickness of the rat's thigh, taking into account the indentation of the cryoapplicator tip.

This result indirectly confirms our assumption about the hemispherical shape of the freeze volume and matching of the radial temperature distribution on the ice spot surface and in ice volume.

The Table demonstrates that the ratio of maximal diameters of necrosis to ice spots for two different cryoablation durations (0.5 and 1 min) is constant 0.64 ± 0.03. Thus, the necrosis volume is about a quarter of the ice hemisphere volume. This result is consistent, for example, with the reported studies [11], where the volume of liver necrosis caused by cryoinjury was assessed by MRI.

Identical ratios of the diameters of necrosis and ice spots at two different durations of rapid freezing confirm the assumption that the instantaneous thermal field in the frozen zone is determined only by the tissue thermophysical parameters. Thus the immediate necrosis volume can be unequivocally estimated by the size of surface ice spot at the same moment. This result suggests that the primary necrosis zone with $T_{nec} \leq -20$ °C can be intraoperatively controlled using any commercial infrared camera with a standard range of measured temperatures (when using such a device, anatomical zone and cryoexposure duration). However, we can hardly state the same for the 2 min' cryoexposure, since thermodynamic conditions have changed as a result of the thigh freezing through (the ice front propagation in depth was stopped). We plan to check the synchronous movement of the ice front and low-temperature isotherms (for example, T = −40 °C) on thicker tissues and with longer cryoexposure.

3.3. Temperature dynamics in QSS

To understand the phenomenon of linear growth of T_{min} during the QSS while the ice spot diameter is constant, we considered the dynamics of the temperature distribution during this stage.

Three the same temperature profiles drawn through the ice spot center at different moments of the QSS (in 1, 3, and 5 min after the stage beginning) for one of the animals after 1 min cryoexposure are shown in Fig. 6.

The dotted line points the ice spot boundary (T = 0°C). There is zoomed part of graph of the temperature "bell" (T ≤ 0 °C) inside the Figure. The corresponding animal's thermal image and temperature profile position are shown in Fig. 2.

We can see that three equally located temperature profiles taken at 2 min intervals coincide. It means that the temperature distribution remains practically unchanged in the quasi-stable stage, excepting slight heating of the central part of the temperature "bell" (see zoomed area). The authors suggest this heating is superficial only and does not reflect structural rearrangement process inside the ice hemisphere.

3.4. Thermal symmetry distortion

When cryoablation is carried out with applicator, it is critical to ensure reliable uniform contact of the instrument working surface with pathological neoplasm throughout the entire cryoexposure. The proper contact can be complicated by anatomical features of neoplasm and its location, as well as human factor in providing the quality control.

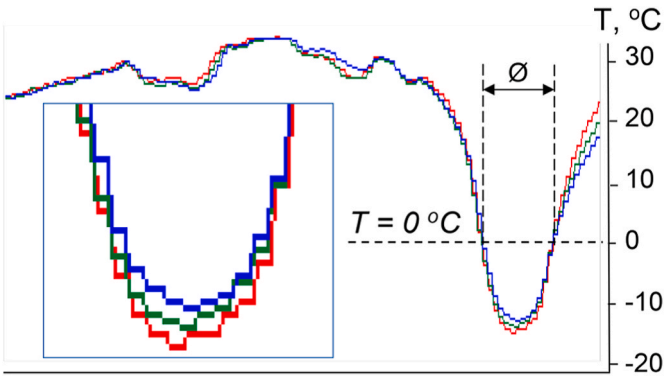

Fig. 6. Temperature profiles through the ice spot center at different moments of the QSS. There is enlarged top of the temperature "bell" in the zoomed area.

In cryosurgery real-time, the IR thermal imaging makes it possible to objectively evaluate the thermal symmetry distortion of ice or necrosis spot. Thermal distortion can be caused by large blood vessel located in target area [3] or other reasons, including the uneven contact of the applicator surface with biological tissues. The corresponding example is shown below. The temperature profiles drawn through the ice spots on skin of two animals 3 s after the ending the 0.5 min' cryoablation, are represented in Fig. 7: (a) without thermocouple, (b) thermocouple located earlier at a distance of 2 mm from the applicator edge, was removed before thermal imaging. The zoomed fragments show the fragments of the corresponding thermal images of ice spots, on which the areas with a temperature of T ≤ −40 °C is colored red. A straight line indicates the thermal profile position, and a circle indicates the previous thermocouple position. The thermal image (b) shows the distortion of the thermal field symmetry and a significant decrease in the area with a temperature of T ≤ −40 °C compared to the thermal image (a). Temperature profile (b) demonstrates quantitative distortion parameters.

However, calculated heat input along two 1 m long wires of the thermocouple used in our study, even with a maximal temperature gradient does not exceed 100 mW.

With such a heat gain, the maximum heating of the surface spot where the thermocouple is placed does not exceed 1 °C. Therefore, the observed significant thermal symmetry distortion cannot be caused by the thermocouple. Also there is no large vessel in this area. This example illustrates the disadvantages of subjective control of the contact of applicator with skin. In our opinion, the distortion of the temperature field (Fig. 7 (b)) was caused by an unconscious cryoinstrument minor deviation from the vertical because of the fear to damage the thermocouple during cryoexposure. As a result, an uneven contact of the applicator working surface with the skin surface significantly affected the temperature distribution in tissues.

3.5. Temperature control of other skin areas

Owing to the capability of thermal imaging to simultaneously monitor the entire thermal field of the animal, it was possible to detect a rapid decrease in temperature by 2–4 °C on skin of other (control) limb at the beginning of cryoexposure. Since the temperature level on the control limb skin did not change when cooling continues and did not depend on the exposure duration, the authors attribute this effect to spasm of the skin vessels. During warming, the control area temperature was slowly restored.

4. Conclusions

1. Infrared imaging is likely shown to be experimentally used to quantitatively control the biological tissue freezing and thawing *in vivo*, including real time control of the necrotic and cryoscopic isotherm position, ice spot thermal symmetry distortion, thermal response of other skin areas.
2. Prolongation of cryoexposure duration from 0.5 to 2 min has been found to lead to proportional increase in amplitude and time parameters of thermal fields on animal's skin during both freezing and subsequent natural warming. The exceptions are the time and temperature of the quasi-stable stages beginning post 2 min cryoexposure, which we explain by the change in thermodynamic equilibrium conditions when the thigh tissue freezes all through.
3. The isomorphism of the dynamics of ice spot diameter and temperature of its center is shown under cryoexposure of different durations. During natural warming, the quasi-stable stages in both dynamics are present, which is apparently associated with structural ice rearrangements in the frozen tissue volume.
4. It has been found that the ratio of the maximum diameters of primary necrosis to ice spots was the same (0.64 ± 0.03) for two durations of cryoexposure. This result opens up the prospects to real time control

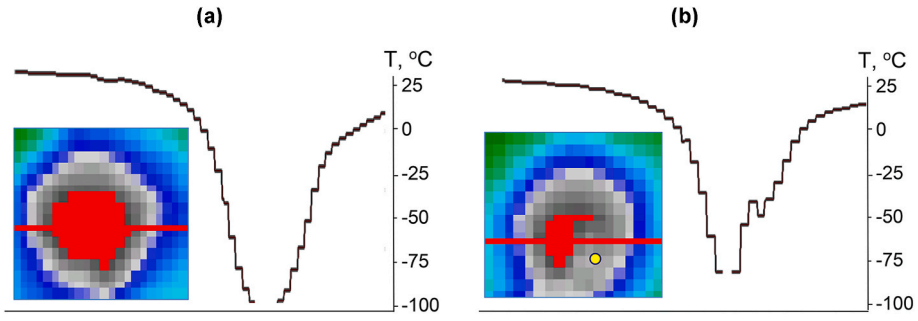

Fig. 7. Temperature profiles through ice spots on the skin of two animals 3 s later the termination of 0.5-min cryoapplication: a) without thermocouple, b). thermocouple located earlier at a distance of 2 mm from the applicator edge, was removed before thermal imaging.

the boundary of the primary necrosis zone of biological tissue measuring the ice spot boundary. That makes it possible to use for this purpose IR cameras with a standard (up to −20 °C) range of measured negative temperatures.

We are keen to continue research *in vitro* and *in vivo* using other biological tissues, as well as with additional methods to assess the volume and shape of the necrosis and ice zones.

Authors' contributions

This research was coined and designed by Gennadiy O. Kovalov and Galyna V. Shustakova. Gennadiy O. Kovalov prepared the animals to cryoablation and fulfilled all manipulations with animals. Eduard Yu. Gordiyenko designed the IR camera targeted to this research task, as well as performed IR imaging. Galyna V. Shustakova quantitatively processed thermal data array. Yuliya V. Fomenko calibrated and tested the IR camera as well as statistically processed thermal data. Mykola I. Glushchuk supervised the research.

Funding

This work was supported by the National Academy of Sciences of Ukraine funding by the grant 0121U108515 titled as "Development of thermal imaging equipment and methods to monitor the temperature fields on human skin in treatment of soft tissue pathologies and to control low-temperature effects on biological tissues".

Declaration of competing interest

None.

References

[1] W. Abramovits, G. Graham, Ya Har-Shai, R. Strumia, Dermatological Cryosurgery and Cryotherapy, Springer, London, 2016, https://doi.org/10.1007/978-1-4471-6765-5.
[2] V. Aquilanti, N.D. Coutinho, V.H. Carvalho-Silva, Kinetics of low-temperature transitions and a reaction rate theory from non-equilibrium distributions, Philos. Trans. A Math. Phys. Eng. Sci. 375 (2017) 20160201, https://doi.org/10.1098/rsta.2016.0201.
[3] Z.-S. Deng, J. Liu, H.-W. Wang, Disclosure of the significant thermal effects of large blood vessels during cryosurgery through infrared temperature mapping, Int. J. Therm. Sci. 47 (2008) 530–545, https://doi.org/10.1016/j.ijthermalsci.2007.05.007.
[4] N.A. Diakides, J.D. Bronzino, Medical Infrared Imaging, CRC Press, New York, 2007.
[5] A.A. Gage, J.A. Caruana Jr., G. Garamy, A comparison of instrument methods of monitoring freezing in cryosurgery, J. Dermatol. Surg. Oncol. 9 (1983) 20–214, https://doi.org/10.1111/j.1524-4725.1983.tb00789.x.
[6] N.E. Hoffmann, J.C. Bischof, Cryosurgery of normal and tumor tissue in the dorsal skin flap chamber: Part I–thermal response, J. Biomech. Eng. 123 (2001) 301–309, https://doi.org/10.1115/1.1385838.
[7] N.N. Korpan, S.G. Chefranov, Estimation of the stable frozen zone volume and the extent of contrast for a therapeutic substance, PLoS One 15 (2020), e0238929, https://doi.org/10.1371/journal.pone.0238929.
[8] G.O. Kovalov, E.Yu Gordiyenko, Yu V. Fomenko, et al., Dynamics of freezing and warming of soft tissues with short-term effect on skin with cryoapplicator, Probl. Cryobiol. Cryomed. 30 (2020) 359–368, https://doi.org/10.15407/cryo30.04.359.
[9] P. Laugier, E. Laplace, J.-I. Lefaix, G. Berger, In vivo results with a new device for ultrasonic monitoring of pig skin cryosurgery: the echographic cryoprobe, J. Invest. Dermatol. 111 (1998) 314–319, https://doi.org/10.1046/j.1523-1747.1998.00288.x.
[10] N.W. Lutz, V. Bernard, Contactless thermometry by MRI and MRS: advanced methods for thermotherapy and biomaterials, iScience 23 (2020), e101561, https://doi.org/10.1016/j.isci.2020.101561.
[11] N. Mala, E. Samset, L. Aurdal, O. Soreide, Magnetic resonance imaging-estimated three-dimensional temperature distribution in liver cryolesions: a study of cryolesion characteristics assumed necessary for tumor ablation, Cryobiology 43 (2001) 268–275, https://doi.org/10.1006/cryo.2001.2351.
[12] C.G. Overduin, J.J. Fütterer, T.W.J. Scheenen, 3D MR thermometry of frozen tissue: feasibility and accuracy during cryoablation at 3T, J. Magn. Reson. Imag. 44 (2016) 1572–1579, https://doi.org/10.1002/jmri.25301.
[13] P. Pasquali, Cryosurgery A Practical Manual, Springer-Verlag, Berlin, Heidelberg, 2015, https://doi.org/10.1007/978-3-662-43939-5.
[14] M.A. Pogrel, C.K. Yen, R. Taylor, A study of infrared thermographic assessment of liquid nitrogen cryotherapy, Oral. Surg. Oral. Med. Oral. Pathol. Oral. Radiol. 81 (1996) 396–401, https://doi.org/10.1016/S1079-2104(96)80014-X.
[15] N.S. Ravikumar, R. Kane, B. Cady, et al., Hepatic cryosurgery with intraoperative ultrasound monitoring for metastatic colon carcinoma, Arch. Surg. 122 (1987) 403–409. https://doi:10.1001/archsurg.1987.01400160029002.
[16] J.C. Rewcastle, G.A. Sandison, L.I. Hahn, et al., A model for the time-dependent thermal distribution within an iceball surrounding a cryoprobe, Phys. Med. Biol. 43 (1998) 3519–3534, https://doi.org/10.1088/0031-9155/43/12/010.
[17] M.J. Taylor, B.P. Weegman, S.C. Baicu, S.E. Giwa, New approaches to cryopreservation of cells, tissues, and organs, Rev. Transfus. Med. Hemother. 46 (2019) 197–215, https://doi.org/10.1159/000499453.
[18] V. Yefremenko, E. Gordiyenko, G. Shustakova, et al., A Broadband imaging system for research applications, Rev. Sci. Instrum. 80 (2009), e056104, https://doi.org/10.1063/1.3124796.
[19] A.I. Zhmakin, Fundamentals of Cryobiology. Physical Phenomena and Mathematical Models, Springer-Verlag, Berlin, Heidelberg, 2009, https://doi.org/10.1007/b10800.
[20] E.E. Zimmerman, P. Crawford, Cutaneous cryosurgery, Am. Fam. Physician 86 (2012) 1118–1124. https://www.aafp.org/afp/2012/1215/p1118.html.